Supramolecular Chemistry
Publication details, including instructions for authors and subscription information:
http://www.informaworld.com/smpp/title~content=t713649759

Selective Recognition of Thallium(I) by *1,3-alternate* Calix[4]arene-bis(crown-6 Ether): A New Talent of the Known Ionophore

Ebony D. Roper[a]; Vladimir S. Talanov[a]; Raymond J. Butcher[a]; Galina G. Talanova[a]
[a] Department of Chemistry, Howard University, Washington, DC, USA

To cite this Article Roper, Ebony D. , Talanov, Vladimir S. , Butcher, Raymond J. and Talanova, Galina G.(2008) 'Selective Recognition of Thallium(I) by *1,3-alternate* Calix[4]arene-bis(crown-6 Ether): A New Talent of the Known Ionophore', Supramolecular Chemistry, 20: 1, 217 — 229
To link to this Article: DOI: 10.1080/10610270701803074
URL: http://dx.doi.org/10.1080/10610270701803074

Supramolecular Chemistry, January–March 2008 Vol. 20 (1–2), pp. 217–229

Taylor & Francis
Taylor & Francis Group

Selective Recognition of Thallium(I) by *1,3-alternate* Calix[4]arene-bis(crown-6 Ether): A New Talent of the Known Ionophore

EBONY D. ROPER†, VLADIMIR S. TALANOV‡, RAYMOND J. BUTCHER¶ and GALINA G. TALANOVA*

Department of Chemistry, Howard University, 525 College Street NW, Washington, DC 20059, USA

Dedicated to Professor David N. Reinhoudt

1,3-Alternate **calix[4]arene-bis(crown-6) (1), designed originally for selective separation of Cs^+ from other alkali metal cations, has been found to possess even higher affinity for a soft electron acceptor Tl^+. Thallium(I) picrate is extracted by 1 from an aqueous solution into chloroform in 1:1 metal-to-ligand stoichiometry, with the extraction constant being 10-fold higher than that found for the extraction of caesium(I) picrate under otherwise identical conditions. The coordination mode of Tl^+ in its complex with 1 in solution has been probed by ^1H NMR ($CDCl_3$) and compared with the analogous complexes of Rb^+ and Cs^+. In addition, X-ray crystal structures of the dinuclear complexes of 1 with TlPic, RbPic and CsPic have been determined. As evident from the structural data in solution and solid state, π-coordination of Tl^+ with the calixarene aromatic framework of 1 plays an important role in the enhanced complexing ability of the calix-biscrown towards this metal ion.**

Keywords: thallium(I); *1,3-alternate* calix[4]arene-bis(crown-6); extraction selectivity; π-coordination; solution and crystal structures

INTRODUCTION

Thallium compounds find numerous applications in technology, science and medicine. However, Tl^+ is extremely toxic, in part because in biological systems it behaves similar to alkali metal cations (AMC). This makes thallium a hazardous anthropogenic pollutant the levels of which in the environment must be controlled. Therefore, development of new reagents and methods for efficient detection and selective removal of Tl^+ has been continuously attaining efforts of scientists.

During the last two decades, calixarene derivatives have occupied an important place among the synthetic macrocyclic ligands employed in metal ion recognition and separations [1,2]. One of the distinctive features of these ionophores is their capability of cation–π interactions involving the aromatic framework [3]. Recently [4–6], this property of calixarene-based ligands (mostly in the *cone* conformation) was found advantageous for complexation of a soft electron acceptor Tl^+. The enhanced affinity towards Tl^+ could be expected from *1,3-alternate* calix[4]arene derivatives as well, since this ligand conformation possesses a recognised potential for cation–π interactions [7]. In particular, Cs^+–π coordination, demonstrated first for *1,3-alternate* calix[4]arene-crown-6 [8,9] and afterwards for the -bis(crown-6) ionophores (e.g. **1**) [10,11], is an important contributing factor in the famous high selectivity of these ligands towards caesium ion over other AMC. Such a unique propensity determined the practical application of this class of ionophores in nuclear waste treatment [12,13] (for examples of Cs^+ separations by **1** and its derivatives, see also [14–18]. However, no information on Tl^+ complexation with *1,3-alternate* calix[4]arenes or their crown ether (CE) derivatives was available until the recent report by our group of a selective determination of both thallium(I) and caesium(I) by a proton-ionisable calix-biscrown **2** containing one pendent dansylcarboxamide group [19].

*Corresponding author. E-mail: gtalanova@howard.edu
†E-mail: e5d5r5@msn.com
‡E-mail: vstalanov@msrce.howard.edu
¶E-mail: rbutcher@howard.edu

ISSN 1061-0278 print/ISSN 1029-0478 online © 2008 Taylor & Francis
DOI: 10.1080/10610270701803074

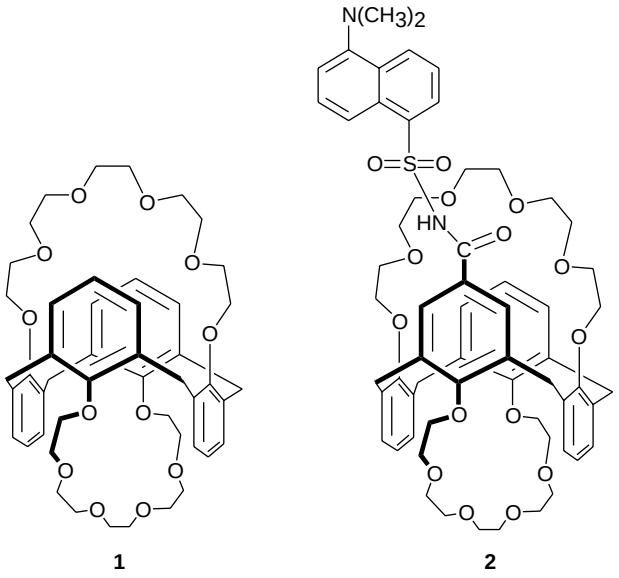

CHART 1

Compound **2** exhibited a high sensitivity towards thallium(I) in the presence of a large excess of different other metal cations [19]. Interestingly, Tl^+ was also found to form a significantly more stable 1:1 complex with ionised **2** than Cs^+. However, due to unavailability of the corresponding published data, it was not obvious whether Tl^+ selectivity of **2** was the propensity inherited from the non-ionisable prototype **1** or whether it was a distinctive property of **2** arising from the presence of dansylcarboxamide side arm adjacent to the calixarene cavity. Such information could be useful for the design of new calixarene-based receptors of thallium(I) ion. Therefore, herein we report the results of Tl^+ recognition by **1** in solvent extraction in comparison with the data obtained for other uni-charged metal cations. Structural studies of Tl^+, Cs^+ and Rb^+ complexes of **1** in solution by ^{1}H NMR and in solid state by single crystal X-ray diffraction are also presented.

RESULTS AND DISCUSSION

Unique complexation characteristics of calix[4]arene-crown-6 type ligands preorganised in *1,3-alternate* conformation evolve from their abilities for size discrimination and π-coordination of metal ions [20]. These ionophores offer oxygen donor atoms appropriate for binding of hard cations as well as π-basic aromatic cavity attractive for soft electron acceptors. Taking into account all of these aspects, **1** is anticipated to be a suitable receptor for Tl^+ as well as Cs^+. As mentioned above, Tl^+ is known for its tendency for π-interactions with calixarene aromatic framework. At the same time, it forms stable complexes with CEs (in particular, with 18-crown-6 derivatives; [21]). In addition, the ionic radius of Tl^+(1.44 Å by Pauling [22]) is almost equal to that of Rb^+(1.48 Å), the principal competitor of Cs^+ in complexation with **1** and its derivatives, which suggests a good geometric fit between the macrocyclic ligand and thallium ion.

SOLVENT EXTRACTION STUDIES

The complexation ability of **1** towards Tl^+ was studied by means of extraction of thallium picrate from aqueous solutions into chloroform. For comparison purposes, extraction of Li^+, Na^+, K^+, Rb^+ and Cs^+ as well as Ag^+ picrates[1] was examined under the otherwise identical conditions. It should be noted at this point that unlike for Tl^+, the extraction propensities of **1** and its derivatives towards AMC were investigated in great detail [14–18]. Also, in view of cation–π coordination capabilities of **1**, its binding of a soft electron-acceptor Ag^+ was tested [24]. However, in contrast with Cs^+, solvent extraction of a relatively small Ag^+ by **1** was distressed by the lack of the ligand donor centre cooperation observed in the structure of $AgNO_3$ complex with **1**. The above phenomenon illustrated again the importance of both of the factors, electronic characteristics and geometric fit, for recognition of a metal ion by *1,3-alternate* calix[4]arene-bis(crown-6).

The results obtained for single-ion solvent extraction of Tl^+, AMC and Ag^+ picrates from 0.10 mM aqueous solutions into chloroform by 1.0 mM **1** are presented in Fig. 1. As evident from this plot, Tl^+ separation by **1** is the most efficient, and the percent extraction of TlPic is significantly higher than that for all other metal ions, including Cs^+. For these extractions, variation of the metal ion distribution ratio, *d* (defined as the ratio of equilibrium concentration of picrate in the organic and the aqueous phases), with the Pauling's ionic radius is shown in Fig. 1b. For nearly the same size cations, Tl^+ and Rb^+, d_{Tl} is about five times as large as d_{Rb} under identical experimental conditions. Such a difference in the efficiency of extraction of these two metal ions by **1** is attributed to the expressed affinity of Tl^+ for cation–π coordination with aromatic calixarene framework.

[1]Earlier [23], we demonstrated that the extraction selectivities of benzo-substituted CEs for AMC may be affected by the picrate anion due to the Pic^--ligand π–π interactions. However, no 'picrate effect' on the metal extraction by **1** is envisioned, since no evidence of π–π stacking of Pic^- with the calixarene aromatic units is found in the crystal as well as solution structures of the corresponding picrate complexes *vide infra*.

For **1** containing two equivalent CE loops, an interaction with uni-charged metal ions (M^+) may result in the formation of complexes with both 1:1 and 2:1 metal-to-ligand stoichiometry [10]. Thus, for Cs^+, Na^+ and Ag^+ complexation with **1**, existence of 2:1 species was observed in solutions and confirmed by X-ray analysis of the corresponding solid complexes. In low-polarity media, complexation of metal salts with neutral ligand **1** proceeds via ion pairing. Accordingly, solvent extraction of metal picrates by **1** may be described by the following equilibria with the corresponding extraction constants, K_{ex}:

$$M^+_{aq} + Pic^-_{aq} + \mathbf{1}_{org} \rightleftharpoons M^+\mathbf{1}Pic^-_{org} \quad (1)$$

$$K_{ex} = \frac{[M^+\mathbf{1}Pic^-]_{org}}{[M^+]_{aq}[Pic^-]_{aq}[\mathbf{1}]_{org}} \quad (2)$$

or

$$2M^+_{aq} + 2Pic^-_{aq} + \mathbf{1}_{org} \rightleftharpoons (M^+)_2\mathbf{1}(Pic^-)_{2\,org} \quad (3)$$

$$K'_{ex} = \frac{[(M^+)_2\mathbf{1}(Pic^-)_2]_{org}}{[M^+]^2_{aq}[Pic^-]^2_{aq}[\mathbf{1}]_{org}} \quad (4)$$

With account for $[M^+]_{aq} = [Pic^-]_{aq}$, equation (2) for the 1:1 extraction stoichiometry may be easily transformed into the linear equation (5):

$$\log D = \log K_{ex} + \log [\mathbf{1}]_{org} \quad (5)$$

$$\text{where} \quad D = \frac{[M^+\mathbf{1}Pic^-]_{org}}{[Pic^-]^2_{aq}} \quad (6)$$

In the case of 1:1 extraction, the plot of log D vs. log $[\mathbf{1}]_{org}$ is linear with a slope of 1 and intercept at the OY axis being equal to log K_{ex}. equation (4) for the 2:1 extraction stoichiometry may be linearised in a similar fashion.

It is worth mentioning that although the ability of **1** and its derivatives to form 2:1 metal complexes is generally recognised, the reports published by different groups of scientists disagree concerning

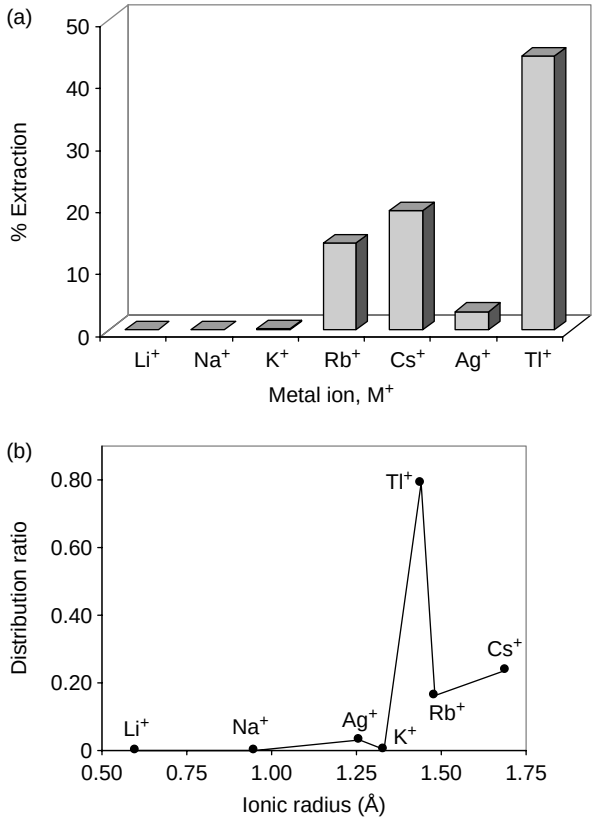

FIGURE 1 Extraction of Tl^+, AMC and Ag^+ picrates from aqueous solutions into chloroform by **1**: (a) variation of the percent extraction with metal ion identity and (b) metal ion distribution ratio as a function of ionic radius. $C_{MPic} = 0.10$ mM and $C_1 = 1.0$ mM.

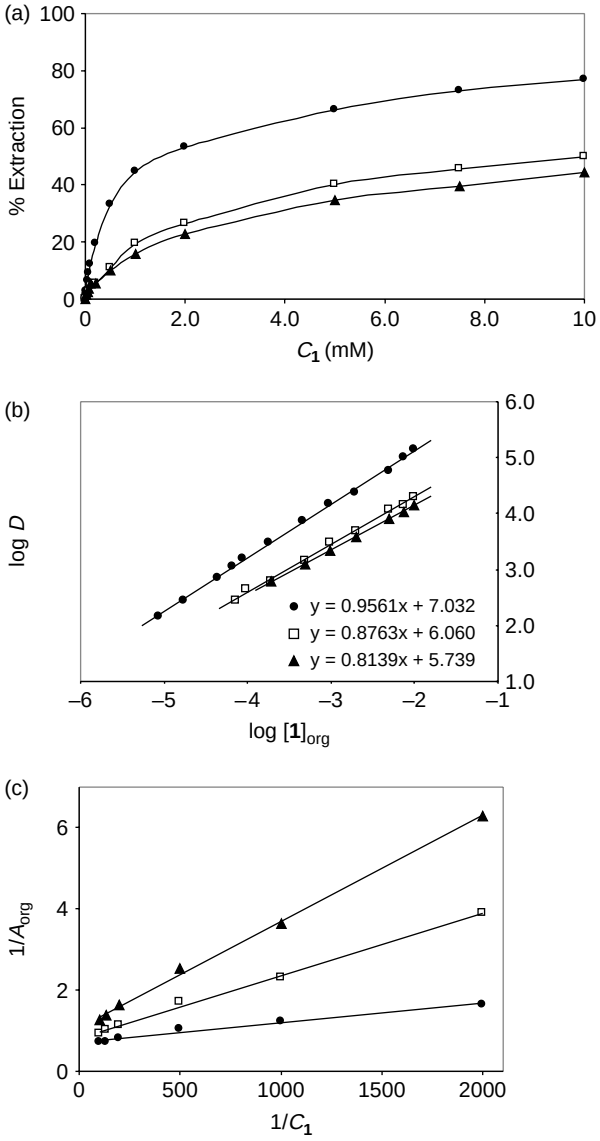

FIGURE 2 Extraction of TlPic, CsPic, and RbPic from 0.10 mM aqueous solutions into chloroform by **1**: (a) changes in the percent extraction of Tl^+(●), Cs^+(□) and Rb^+(▲) with varying concentrations of the ligand in the organic phase, C_1; (b) the plots of log D vs. log $[\mathbf{1}]_{org}$ and (c) the plots of $1/A_{org}$ vs. $1/C_1$.

TABLE I Chemical shifts for the methylene group protons in the ^{1}H NMR spectra (400 MHz, 293 K) of **1** and its dinuclear complexes with TlPic, RbPic and CsPic in $CDCl_3$.

	δ, ppm					
Compound/protons	*a* (s, 8H)	*b* (t, 8H)	*c* (t, 8H)	*d* (t, 8H)	*e* (t, 8H)	*f* (s, 8H)
1	3.71	3.65	3.48	3.60	3.33	3.82
	$\Delta\delta$, ppm					
Tl_2**1**$(Pic)_2$	−0.03	0.11	0.35	0.33	0.53	−0.08
Rb_2**1**$(Pic)_2$	−0.11	~0.04	~0.28	~0.30	~0.46	−0.05
Cs_2**1**$(Pic)_2$	−0.11	0.03	0.27	0.29	0.46	−0.04

the factual occurrence of the dinuclear complexes of such ligands in solvent extraction. Thus, Vicens *et al.* [10] concluded that in solutions containing water, in particular, in the extraction systems (e.g. water–dichloromethane, NPOE or NPHE; [14–16]), 1:1 complex is the only species formed by **1** with Cs^+, supposedly due to hydration of the potential binding site for the second metal cation. The 1:1 metal-to-**1** extraction stoichiometry was also reported for other AMC [14] and Ag^+[24]. Similarly, our earlier studies of solvent extraction of AMC by proton-ionisable mono-*N*-(X-sulphonylamide) analogues of **1** [18] showed no indication of 2:1 metal-to-ligand complexation. On the other hand, Moyer and co-workers [17] demonstrated that the results of $CsNO_3$ extraction by calix[4]arene-bis(*t*-octylbenzo-crown-6) from water into dichloroethane were consistent with formation of both 2:1 and 1:1 complex species.

Therefore, it was interesting to determine TlPic-**1** complex stoichiometry and extraction constant in the water–chloroform system and compare these data with the behaviour of RbPic and CsPic under the same conditions. To this end, extractions of the three metal picrates from 0.10 mM aqueous solutions into chloroform with varying concentrations of **1** were studied. The plots for the dependence of the percent extraction of TlPic, CsPic and RbPic on the formal concentration of the ligand in the organic phase, $C_{\mathbf{1}}$, are presented in Fig. 2(a). As may be seen in Fig. 2(b), these extraction data give linear plots in the coordinates of log D vs. log $[\mathbf{1}]_{org}$ for a wide range of $C_{\mathbf{1}}$, which is consistent with 1:1 metal-to-**1** stoichiometry (equation (5)). Linear are also the double-reciprocal graphs of $1/A_{org}$ vs. $1/C_{\mathbf{1}}$ (where A_{org} is the absorbance of picrate in chloroform) for the extraction of TlPic, CsPic and RbPic by **1** in the concentration region of $C_{\mathbf{1}} > C_{MPic}$, so that $[\mathbf{1}]_{org} \rightarrow C_{\mathbf{1}}$ (Fig. 2(c)). Therefore, under the applied experimental conditions, 1:1 complex is the dominant extracted species for these three metal picrates. The extraction constants, log K_{ex}, determined from the linear plots in Fig. 2(b) are 7.03, 6.06 and 5.74 for Tl^+, Cs^+ and Rb^+, respectively.

^{1}H NMR STUDY OF TLPIC, CSPIC AND RBPIC COMPLEXES OF 1

To probe for any peculiarities in the coordination mode of Tl^+ with **1** in solution, complexation-induced changes in the ^{1}H NMR spectrum of the calix-biscrown in the presence of TlPic in $CDCl_3$ were examined in comparison with those for RbPic and CsPic. The dinuclear complexes, Tl_2**1**$(Pic)_2$, Rb_2**1**$(Pic)_2$ and Cs_2**1**$(Pic)_2$, were synthesised, dissolved in $CDCl_3$ and their ^{1}H NMR spectra recorded. It should be mentioned at this point that based on our earlier studies of the 'picrate effect' [23], the magnitude of chemical shifts observed for the singlets of Pic^- protons, $\delta_{Pic} = 8.86$ ppm for Tl_2**1**$(Pic)_2$ and 8.90 ppm for both Rb_2**1**$(Pic)_2$ and Cs_2**1**$(Pic)_2$, did not suggest any significant $\pi-\pi$ Pic^--ligand interactions in these three complexes in $CDCl_3$ solution.

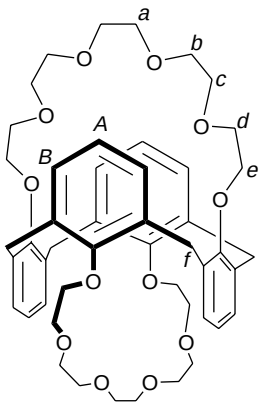

CHART 2

The ^{1}H NMR spectrum for a symmetrical molecule of **1** in the region of 3.30–3.95 ppm (Fig. 3; Table I) contains two pairs of triplets and a singlet produced by the methylene group protons *b–e* and *a*, respectively, of the CE O-CH_2CH_2-O fragments as well as a singlet for Ar-CH_2-Ar protons (*f*) of the *1,3-alternate* calix[4]arene moiety. In the spectra

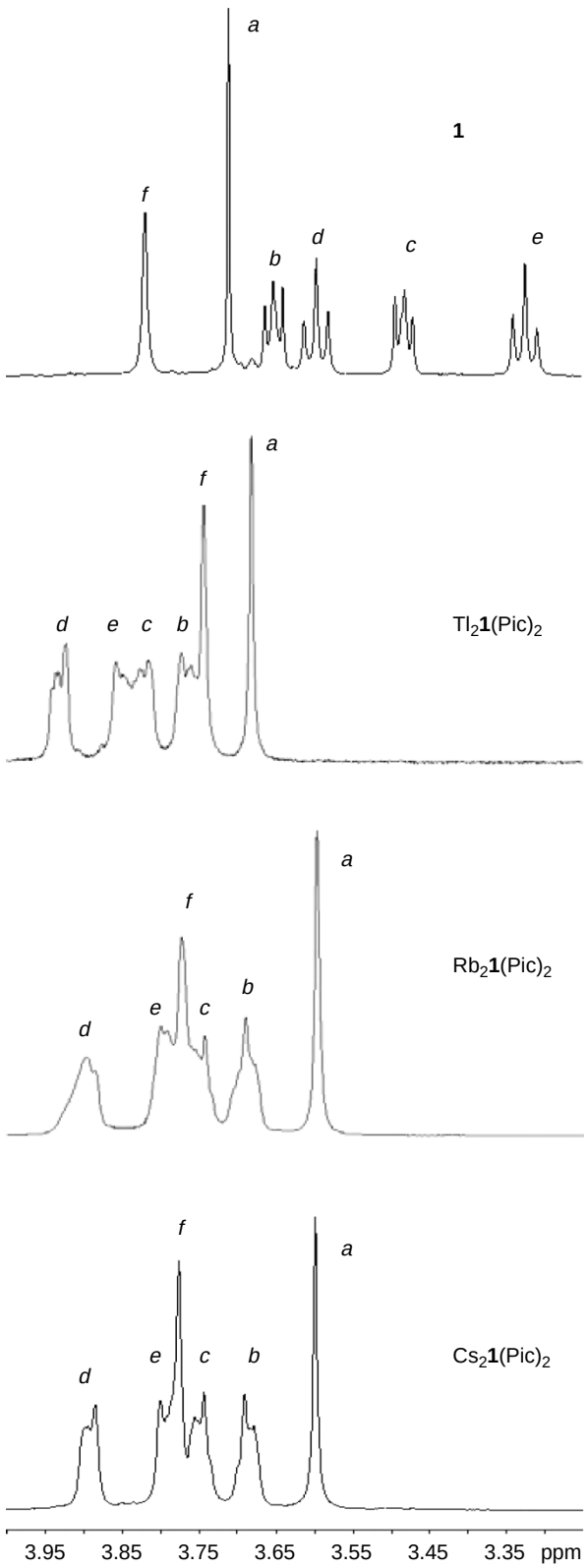

FIGURE 3 ^{1}H NMR spectra (400 MHz, 293 K) for the methylene group protons of **1** and its complexes with TlPic, RbPic and CsPic in $CDCl_3$.

of Tl_2**1**$(Pic)_2$, Rb_2**1**$(Pic)_2$ and Cs_2**1**$(Pic)_2$ in $CDCl_3$, all of these signals showed noticeable shifts ($\Delta\delta$, Table I) relative to those in the spectrum of free **1**[2]. As may be seen in Fig. 3, complex formation also caused a considerable broadening of the triplets for the ligand protons *b*–*e*. This effect is especially strong in the case of Rb_2**1**$(Pic)_2$. Other than that, the ^{1}H NMR spectra of Rb_2**1**$(Pic)_2$ and Cs_2**1**$(Pic)_2$ in this region are similar, while the spectrum of Tl_2**1**$(Pic)_2$ is unique.

The factual changes in the positions of the signals for the ligand O-CH_2CH_2-O protons observed upon complexation of **1** represent an overall effect from different electronic and geometric factors. Thus, variation in the electron environment of the CH_2-group protons due to metal ion coordination by the adjacent oxygen donor atoms produces downfield shifts (positive $\Delta\delta$) of their ^{1}H NMR signals. At the same time, inclusion of M^+ in the cavity of **1** decreases flexibility of the CE loops, limiting significantly the number of conformations they can adopt. In particular, metal coordination inhibits such ligand conformations in which the CE CH_2-groups, particularly protons *a* and *b*, might approach the arene units and get exposed to their shielding effect. This should cause an upfield shift (negative $\Delta\delta$) of the corresponding signals in the ^{1}H NMR spectrum of the complex relative to that for the free **1**. Thus, the electronic and geometric changes which occur in the ligand molecule upon complexation may produce opposite effects on the position of the signals for the CE O-CH_2CH_2-O protons.

As evident from the downfield shifts observed for the corresponding triplets (Fig. 3; Table I), the electronic component is the major contributing factor in the spectral behaviour of protons *c*–*e* in the complexes Tl_2**1**$(Pic)_2$, Rb_2**1**$(Pic)_2$ and Cs_2**1**$(Pic)_2$. The prevalence of electronic over the geometric effects from metal coordination for the protons in the lower part of the CE ring might result from a limited conformational mobility of the O-CH_2CH_2-O fragments neighbouring the rigid calixarene framework. However, for the methylene group protons *a* and *b* located in the upper, mobile part of the CE loop, the increment from the geometric factor (shifting the signals upfield) in the overall ^{1}H NMR spectrum changes due to complex formation must be important. One may see that binding of Tl^+ by **1** produces the largest positive $\Delta\delta$ for protons *c*–*e* and only a minor negative shift for the singlet of protons *a*. On the contrary, the NMR spectra of Cs_2**1**$(Pic)_2$ and Rb_2**1**$(Pic)_2$ show noticeable $\Delta\delta$ for both protons *a* (upfield) and *c*–*e* (downfield). This may indicate that in solution, coordination of Tl^+ by the CE moiety takes place predominantly via the oxygens located

[2] In this work, assignment of the signals for protons *b*–*e* in the spectra of the MPic-complexes of **1** was made based on the published NMR data for the closest analogues [10,18], with account for the *vide infra* crystallographic information for Tl_2**1**$(Pic)_2$, Rb_2**1**$(Pic)_2$ and Cs_2**1**$(Pic)_2$, in particular, the M—O bond distances.

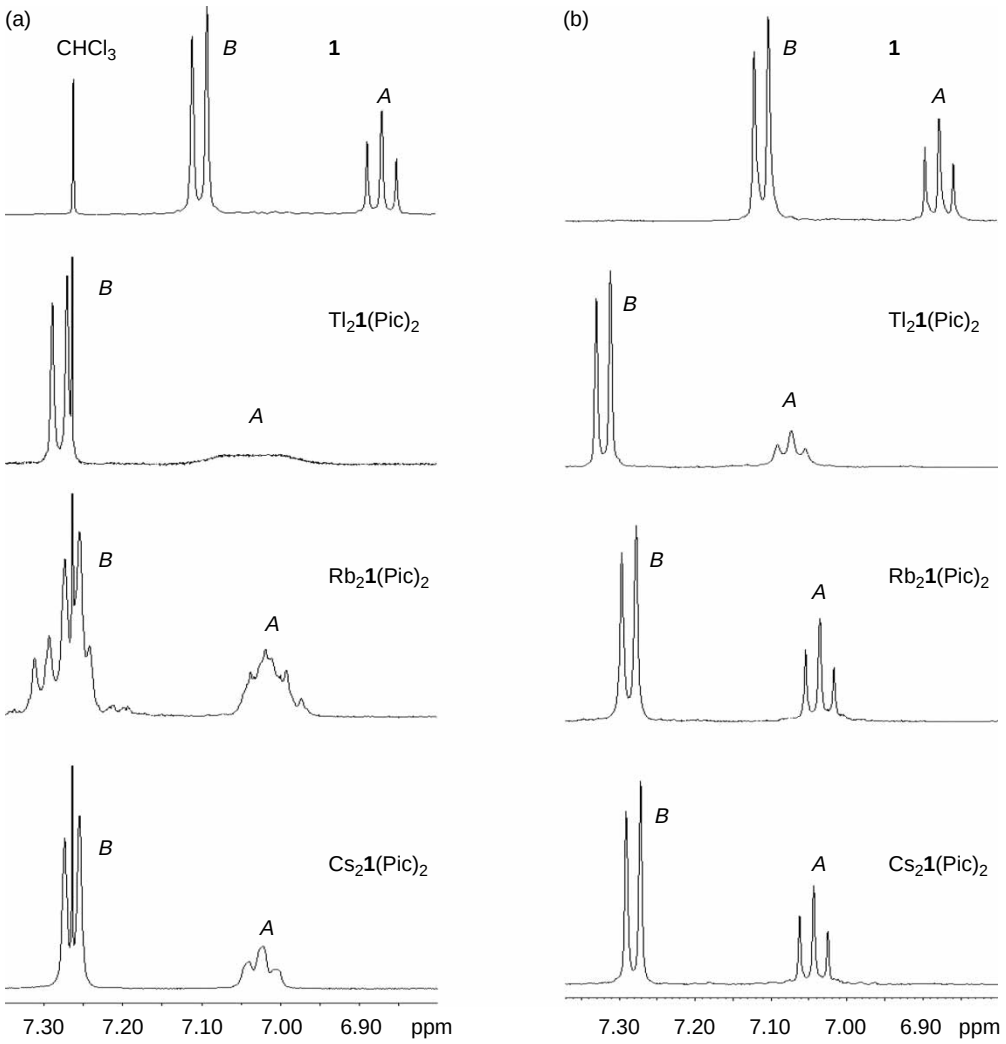

FIGURE 4 ^{1}H NMR spectra (400 MHz, 293 K) for the aromatic protons of **1** and its complexes Tl_2**1**$(Pic)_2$, Rb_2**1**$(Pic)_2$ and Cs_2**1**$(Pic)_2$ in (a) in $CDCl_3$ and (b) $CDCl_3$–CD_3OD (3:1 v/v).

close to the the calixarene moiety, while the oxygen atoms in the remote positions are scarcely involved in the metal ion binding. Therefore, Tl^+ ions must be situated in the bottom parts of the CE loops of **1**, near the calixarene moiety. In contrast, Rb^+ and Cs^+ are bound with all of the donor oxygens of **1** and hence, must be located closer to the centres of the CE rings.

In the molecule of **1**, the four methylene groups *f* bridging the skeletal arene units are remote from the actual metal coordination sites and thus should not experience any direct electronic effects from the complexation. Therefore, a moderate upfield shift observed for the singlet of protons *f* upon metal binding may be attributed entirely to a variation in the conformation of the calixarene moiety. Although, no principal changes in the *1,3-alternate* geometry of rigid **1** with encapsulation of the M^+ are feasible, some deviation in the mutual spatial orientation of the arene units may take place. As obvious from the magnitude of $\Delta\delta$ for protons *f* in Fig. 3 and Table I, this effect is more pronounced in Tl_2**1**$(Pic)_2$ than in Rb_2**1**$(Pic)_2$ and Cs_2**1**$(Pic)_2$. This observation is in agreement with the above assumption of Tl^+ being situated deeper in the calix-crown cavity than Rb^+ and Cs^+.

Because of the envisioned presence of cation–π interactions in Tl_2**1**$(Pic)_2$, Rb_2**1**$(Pic)_2$ and Cs_2**1**$(Pic)_2$, NMR behaviour of the calixarene aromatic protons was of special interest in this study. The ^{1}H NMR spectra in the region of 6.80–7.35 ppm for **1** and its dinuclear MPic-complexes in $CDCl_3$ are shown in Fig. 4(a). It is obvious that in the presence of Tl^+, Rb^+ and Cs^+, a triplet for four protons *A* and a doublet for eight protons *B* of the arene units exhibit downfield shifts, consistent with the effect of cation–π coordination [10]. Along with this general tendency, the following interesting peculiarities in the spectral behaviour of the aromatic protons in these complexes are worth mentioning. In particular, the triplet for protons *A*, unlike the doublet for protons *B*, shows significant broadening upon complex formation. This effect is especially dramatic in the case

TABLE II Chemical shifts for the aromatic protons in the ^{1}H NMR spectra (400 MHz, 293 K) of **1** and its complexes with TlPic, RbPic, and CsPic in $CDCl_3$–CD_3OD (3:1 v/v).

	A (t, 4H)		*B* (d, 8H)	
Compound/protons	δ, ppm	$\Delta\delta$, ppm	δ, ppm	$\Delta\delta$, ppm
1	6.88	–	7.11	–
Tl_2**1**$(Pic)_2$	7.07	0.19	7.32	0.21
Rb_2**1**$(Pic)_2$	7.04	0.16	7.29	0.18
Cs_2**1**$(Pic)_2$	7.04	0.16	7.28	0.17

of Tl_2**1**$(Pic)_2$. As was suggested earlier for Cs^+-complexation with **1** [10], broadening of the signals might result from fast exchange between the 1:1 and 2:1 complex species. However, such an exchange process should affect the width of the doublet for protons *B* as well, which is not observed in the NMR spectra of Tl_2**1**$(Pic)_2$, Rb_2**1**$(Pic)_2$ and Cs_2**1**$(Pic)_2$. In our opinion, another plausible reason for this phenomenon consists of the existing exchange between the complexes with somewhat varying position of the metal ions about the ligand cavity. The appearance of the ^{1}H NMR spectrum for the aromatic protons of Rb_2**1**$(Pic)_2$, which has obvious distinctions from those of the corresponding Tl^+- and Cs^+-complexes, is in agreement with the suggested explanation. As may be seen in Fig. 4(a), coordination of Rb^+ with **1** in $CDCl_3$ solution produced several doublets for the protons *B* rather than one average weighted signal, like that observed for Tl^+ and Cs^+. The same seems to happen to the triplet for protons *A* in this complex. Apparently, the lifetime of several forms of Rb_2**1**$(Pic)_2$ differing in the location of Rb^+ ions about the calixarene moiety and CE loops is long enough for their signals to be observed separately.

For the solvent variation from $CDCl_3$ to $CDCl_3$–CD_3OD (3:1 v/v), sharpness of the signals for the aromatic protons *A* in the NMR spectra of the complexes increased significantly (Fig. 4(b)). In addition, the spectrum of Rb_2**1**$(Pic)_2$ became nearly identical to that of Cs_2**1**$(Pic)_2$. (Interestingly, no improvement in the spectral picture was attained upon saturation of the $CDCl_3$ solutions of the 2:1 complexes of **1** with the corresponding metal picrates.) The $\Delta\delta$ values for the signals of aromatic protons in Tl_2**1**$(Pic)_2$, Rb_2**1**$(Pic)_2$ and Cs_2**1**$(Pic)_2$ in $CDCl_3$–CD_3OD relative to those for the free ligand in the same solvent are listed in Table I. As obvious from these data, coordination of Tl^+ with **1** produces the largest downfield shifts of the signals for the ligand aromatic protons, which indicates the strongest cation–π interactions in this complex. Again, this tendency is in agreement with the above conclusion about Tl^+ residing deeper in the calixarene cavity than Rb^+ and Cs^+. As will be shown below, crystal structures of Tl_2**1**$(Pic)_2$, Rb_2**1**$(Pic)_2$ and Cs_2**1**$(Pic)_2$ are in agreement with the conclusions made for the ^{1}H NMR studies of the three dinuclear complexes in solution.

CRYSTAL STRUCTURES OF DINUCLEAR TL^+, RB^+ AND CS^+ PICRATE COMPLEXES OF 1

X-ray crystal structures for the dinuclear complexes of **1** with $CsNO_3$, CsI and CsNCS were determined and discussed in detail earlier [10,11]. Solid-state structures for K^+, Na^+ [11] and Ag^+ [24] nitrate complexes of this ligand are known as well. However, no crystallographic data for the coordination compounds of **1** with Tl^+ and Rb^+ have been reported to date, to the best of our knowledge. Surprisingly, X-ray structural studies for metal picrate complexes of **1** in general have not been undertaken[3], although, picrates were widely employed in the probing of complexing abilities of this calix-biscrown by solvent extraction.

Therefore, to gain insight into the coordination arrangement of Tl^+ complex with **1** in the solid state and compare it with the corresponding structures for Cs^+ and Rb^+, X-ray quality single crystals of the dinuclear metal picrate complexes, $[Tl_2$**1**$(Pic^-)(CH_3OH)]^+(Pic^-)\cdot CH_3OH$ (**A**), $[Cs_2$**1**$(Pic)_2]$ (**B**) and $[Rb_2$**1**$(Pic)_2]$ (**C**), were obtained and their structures studied by X-ray diffraction. Crystallography data for **A**, **B** and **C** are provided in the Experimental section. Selected bond distances are listed in Table III.

In general features, the coordination arrangement for the metal cations in **A**, **B** and **C** resembles that in the known complexes of Cs^+ with **1** [11] and mono-crown analogues [8,9]. In particular, each of the two CE moieties of the ligand includes a metal ion (Tl^+, Rb^+ or Cs^+) bound with its ether oxygen atoms as well as oxygens of the anion or solvent. In addition, all of the metal ions in these complexes interact with the terminal carbon atoms of the neighbouring arene units in the calixarene framework. However, the crystal structures obtained herein demonstrate a number of distinctive characteristics arising from the properties of the included metal cations (in the case of **A**) as well as Pic^- anion. The discussion below focuses primarily on those structural aspects of **A**, **B** and **C** which, in our opinion, allow to explain the enhanced complexation ability of **1** towards Tl^+ relative to Rb^+ and Cs^+. A more detailed description of the complexes is available in the Supplementary Information.

As mentioned above, the ionic radius of Tl^+ is nearly the same as that of Rb^+, and both of these cations are appreciably smaller than Cs^+.

[3] Crystal structures of CsPic-complexes with the related mono-crown calix[4]arene derivatives in *1,3-alternate* conformation are described in [8,9].

TABLE III Selected bond distances (Å) in the crystal structures of $[Tl_2\mathbf{1}(Pic^-)(CH_3OH)]^+(Pic^-)\cdot CH_3OH$ (**A**), $[Cs_2\mathbf{1}(Pic)_2]$ (**B**) and $[Rb_2\mathbf{1}(Pic)_2]$ (**C**).

	Distances					
Complex	Metal–oxygen (CE)		Metal–carbon (calixarene aromatics)		Metal–oxygen (anion/solvent)	
A	Tl(1)–O(1A)	3.341(4)	Tl(1)–C(3B)	3.466(7)	Tl(1)–O(1P)	2.766(5)
	Tl(1)–O(2A)	3.176(5)	Tl(1)–C(4B)	3.321(7)	Tl(1)–O(16B)	3.639(11)
	Tl(1)–O(3A)	3.453(5)	Tl(1)–C(5B)	3.673(7)	Tl(2)–O(1M)	2.780(8)
	Tl(1)–O(4A)	3.929(5)	Tl(1)–C(19B)	3.235(7)		
	Tl(1)–O(5A)	3.432(5)	Tl(1)–C(20B)	3.124(7)		
	Tl(1)–O(6A)	2.929(4)	Tl(1)–C(21B)	3.558(8)		
	Tl(2)–O(1B)	3.137(4)	Tl(2)–C(3A)	3.387(7)		
	Tl(2)–O(2B)	2.830(5)	Tl(2)–C(4A)	3.089(7)		
	Tl(2)–O(3B)	3.737(5)	Tl(2)–C(5A)	3.288(7)		
	Tl(2)–O(4B)	3.434(5)	Tl(2)–C(19A)	3.730(6)		
	Tl(2)–O(5B)	3.157(5)	Tl(2)–C(20A)	3.470(7)		
	Tl(2)–O(6B)	3.268(4)	Tl(2)–C(21A)	3.719(7)		
B	Cs(1)–O(1A)	3.180(2)	Cs(1)–C(3B)	3.624(4)	Cs(1)–O(1P)	3.141(3)
	Cs(1)–O(2A)	3.093(2)	Cs(1)–C(4B)	3.397(4)	Cs(2)–O(2P)	3.029(2)
	Cs(1)–O(3A)	3.291(2)	Cs(1)–C(5B)	3.662(4)	Cs(2)–O(221)	3.218(3)
	Cs(1)–O(4A)	3.026(2)	Cs(1)–C(19B)	3.572(3)		
	Cs(1)–O(5A)	3.069(2)	Cs(1)–C(20B)	3.319(3)		
	Cs(1)–O(6A)	3.4275(19)	Cs(1)–C(21B)	3.584(3)		
	Cs(2)–O(1B)	3.386(2)	Cs(2)–C(3A)	3.778(3)		
	Cs(2)–O(2B)	3.135(2)	Cs(2)–C(4A)	3.497(3)		
	Cs(2)–O(3B)	3.203(2)	Cs(2)–C(5A)	3.714(3)		
	Cs(2)–O(4B)	3.270(2)	Cs(2)–C(19A)	3.712(3)		
	Cs(2)–O(5B)	4.065(2)	Cs(2)–C(20A)	3.360(3)		
	Cs(2)–O(6B)	3.143(2)	Cs(2)–C(21A)	3.494(3)		
C	Rb(1)–O(1A)	3.483(4)	Rb(1)–C(3B)	3.553(6)	Rb(1)–O(1P)	3.103(5)
	Rb(1)–O(2A)	3.041(4)	Rb(1)–C(4B)	3.289(6)	Rb(2)–O(2P)	3.016(4)
	Rb(1)–O(3A)	3.024(5)	Rb(1)–C(5B)	3.583(6)	Rb(2)–O(262)	3.221(5)
	Rb(1)–O(4A)	3.271(5)	Rb(1)–C(19B)	3.577(6)		
	Rb(1)–O(5A)	3.060(4)	Rb(1)–C(20B)	3.347(6)		
	Rb(1)–O(6A)	3.192(4)	Rb(1)–C(21B)	3.662(6)		
	Rb(2)–O(1B)	3.143(3)	Rb(2)–C(3A)	3.718(6)		
	Rb(2)–O(2B)	4.042(5)	Rb(2)–C(4A)	3.352(6)		
	Rb(2)–O(3B)	3.264(5)	Rb(2)–C(5A)	3.487(6)		
	Rb(2)–O(4B)	3.192(4)	Rb(2)–C(19A)	3.775(6)		
	Rb(2)–O(5B)	3.100(4)	Rb(2)–C(20A)	3.502(6)		
	Rb(2)–O(6B)	3.401(4)	Rb(2)–C(21A)	3.733(6)		

Nevertheless, complexes $[Cs_2\mathbf{1}(Pic)_2]$ and $[Rb_2\mathbf{1}(Pic)_2]$ (structures **B** and **C**, respectively) are isostructural, while $[Tl_2\mathbf{1}(Pic^-)(CH_3OH)]^+(Pic^-)\cdot CH_3OH$ (**A**) is unique. The same tendency was observed for the ^1H NMR spectra of MPic-complexes of **1** in $CDCl_3$ solution presented *vide supra*. Apparently, electronic characteristics of the metal cations, in particular, electron-acceptor properties, have a larger impact on the complex geometry than their sizes.

Due to the possibility of different location of the metal-coordinated anions/solvent about the CE moieties of **1**, complexes **A**, **B** and **C** crystallise as racemic mixtures of enantiomers. For each of these structures, one of the stereoisomers is shown in Figs. 5 and 6 and S1 (Supplementary Information), respectively. The crystal packing for **A**, **B** and **C** is presented in Figs. S2–S4 in the Supplementary Information.

Metal Ion–crown Ether Interactions

It is important to point out that in both **B** and **C**, metal ion M(1) is coordinated with the monodentate Pic^- (via the phenol oxygen) and M(2) is bound with the bidentate anion. Based on this feature, **B** and **C** resemble one of the two earlier published dinuclear $CsNO_3$-complexes of **1**, $Cs_2\mathbf{1}(NO_3)_2$ [10] (referred *vide infra* as structure **D**), which includes the monodentate and bidentate NO_3^-. In contrast with **B** and **C** (as well as **D**), in the dinuclear TlPic-complex **A**, Tl(1) is coordinated with the monodentate Pic^-, while Tl(2) is bound with methanol molecule in place of the counter ion (the second Pic^- anion present in this structure is not included in the coordination sphere of Tl(2).) **A** does not have any immediate analogues among the earlier reported Cs^+-complexes of **1**.

In **A** (Fig. 5), Tl(1) and Tl(2) interact with the corresponding CE moieties of **1** in a similar fashion. In both of them, the distances to five out of the six ether oxygen atoms range from 2.830(5) to 3.453(5) Å (mean value 3.2(2) Å). The sixth oxygen atom, O(4A) in crown 1 and O(3A) in crown 2, is located much farther from the corresponding Tl^+ ion than the others. The length of Tl–O separations generally increases from the lower, adjacent to the calixarene moiety, to the upper, remote parts of the polyether

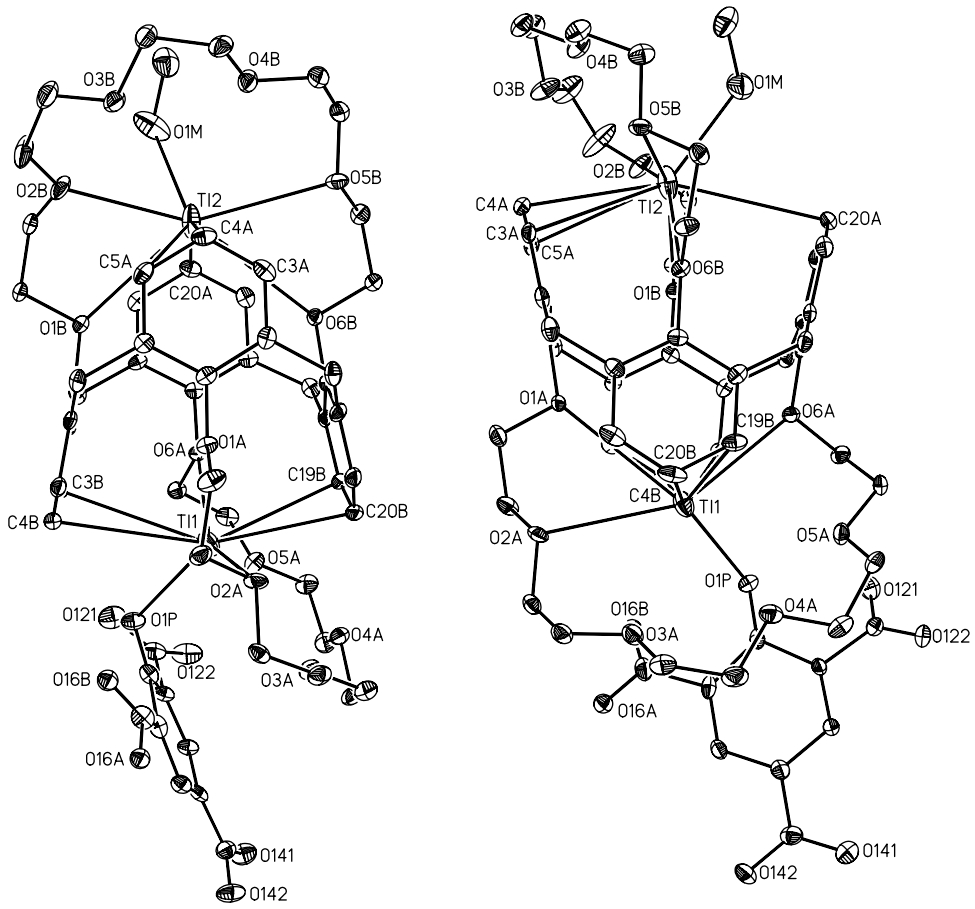

FIGURE 5 Two views of the molecular unit of $[Tl_2\mathbf{1}(Pic^-)(CH_3OH)]^+(Pic^-)\cdot CH_3OH$ (**A**) (hydrogen atoms not shown for clarity).

loops (Table III). Using the sum of the ionic radius for Tl^+ and effective van der Waals radius for O ($s_{Tl-O} = 2.84$ Å) as an indicator for evaluation of the relative bond strength, it may be concluded that each of the thallium ions is coordinated efficiently only with the oxygen atoms situated near the calixarene aromatic cavity. Oxygens in the upper parts of the CEs scarcely interact with Tl^+. Instead, the coordination sphere of Tl(1) includes the phenol atom of the monodentate Pic^-, while Tl(2) is bound with oxygen of methanol molecule. Interestingly, the bond distances of the anion and solvent to the corresponding Tl^+ cations in **A** are noticeably shorter than the separations of these metal ions from the CE oxygens.

In **B** (Fig. 6) and **C** (Fig. S1), the number and spatial arrangement of the CE oxygen atoms around Cs(1) and Rb(1) interacting with the monodentate Pic^- diverge from that for Tl(1) in **A**. These two metal ions are situated near the centres of the corresponding crown 1 loops. Thus, Cs(1) in **B** is coordinated with all six of the polyether oxygens at distances ranging from 3.026(2) to 3.4275(19) Å (mean value 3.2(1) Å). (For comparison, the sum of the Cs^+ ionic radius and effective van der Waals radius for O, s_{Cs-O} is 3.09 Å.) The analogous Rb(1)–O separations in **C** vary from 3.024(5) to 3.483(4) Å (mean value 3.2(2) Å). However, with account for s_{Rb-O} being only 2.88 Å, it may be concluded that interaction of Rb^+ with the CE in **C** must be weaker than that in the isostructural Cs^+-complex **B**. The seventh coordination site at M(1) in these two complexes is occupied by the phenol oxygen of Pic^- at a bond length comparable with the M(1)–O distances for the CE oxygen atoms (Table III).

At the same time, Cs(2) of **B** coordinated with the bidentate Pic^- is bound with only five of the crown 2 oxygen atoms at distances ranging from 3.135(2) to 3.386(2) Å (mean value 3.2(1) Å). The analogous Rb(2)–O separations in **C** vary from 3.100(4) to 3.401(4) (mean value 3.2(1) Å). The sixth polyether oxygen (O(5B) in **B** and O(2B) in **C**) is about 4.0 Å apart. Instead, the coordination sphere of M(2) is completed by two oxygen atoms of the bidentate picrate. In contrast with the Tl^+-containing structure **A**, in **B** and **C**, the counter ion takes place of the ligand oxygen atom located in the lower part of the CE loop.

It should be mentioned at this point that from a comparison of **B** with the analogous $CsNO_3$-complex **D**, it is apparent that the counter-ion variation from NO_3^- to Pic^- has an important effect on the complex crystal structure. In **D**, both Cs1 and

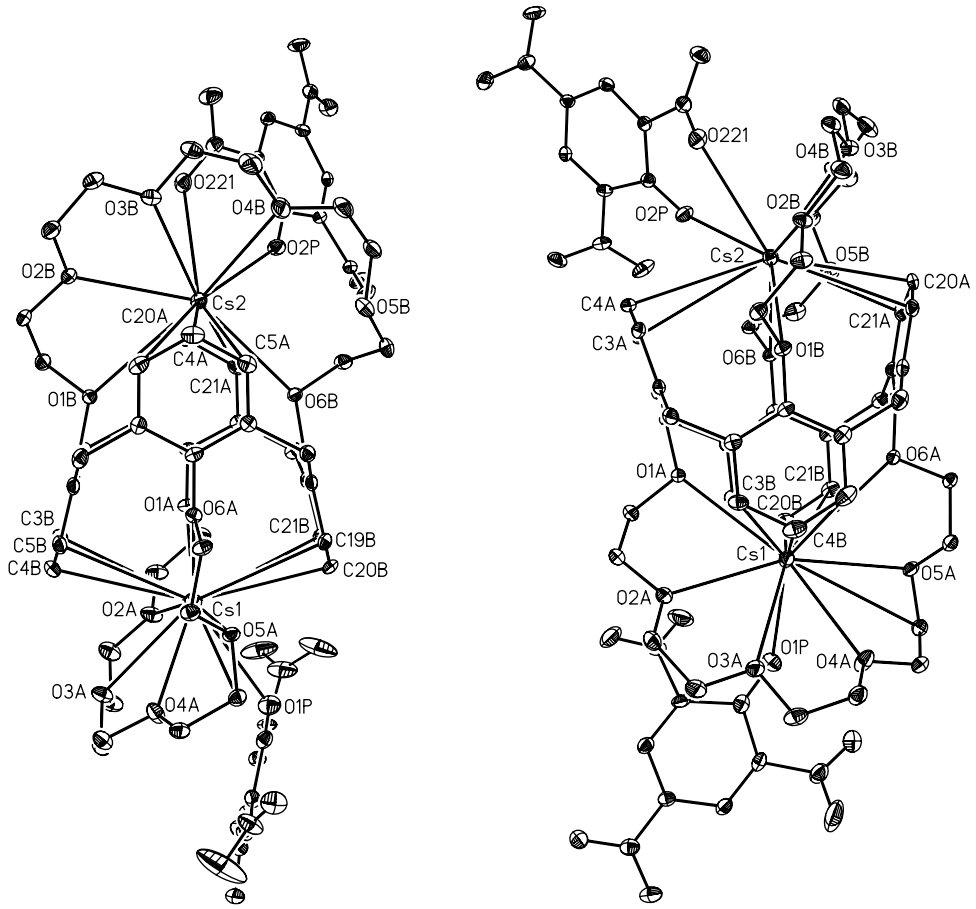

FIGURE 6 Two views of the molecular unit of $[Cs_2\mathbf{1}(Pic)_2]$ (**B**) (hydrogen atoms not shown for clarity).

Cs2 coordinated with the bi- and monodentate nitrate, respectively, are bound with six oxygens of the corresponding crown rings at distances ranging from 3.212(7) to 3.530(8) Å (mean value 3.4(1) Å) for Cs1 and from 3.121(8) to 3.284(8) Å (mean value 3.18(6) Å) for Cs2 [10]. As described above, the similar spatial arrangement of the CE oxygen atoms around Cs^+ ions in **B** is achieved only in the presence of the monodentate Pic^-. Accordingly, conformations of the CE loops in the picrate complex **B** (as well as **C** and **A**) are different from those in **D** [10][4].

Therefore, from the comparison of structure **A** to **B** and **C**, one may find that the location of the metal cations within the ligand polyether loops in these complexes differs. Tl^+ resides closer to the calixarene moiety of **1** than Cs^+ and Rb^+, both of which occupy positions near the CE centres. Evidently, this deviation reflects a stronger affinity of thallium for the cation–π interactions with the aromatic cavity of **1**.

Cation–π Interactions

In **A**, **B** and **C**, similar to the known complexes of Cs^+ with **1** [11] and the related mono-crown ionophores [8,9], each of the metal cations is involved in polyhapto-type interactions with two neighbouring inverted phenol rings of the *1,3-alternate* calix[4]arene moiety of **1** (Figs 5 and 6 and S1). The relevant metal–carbon distances for these structures are listed in Table III. As obvious from these data, the location of Tl^+ ions about the corresponding pairs of aromatic units in **A** differs from those for Cs^+ and Rb^+ in **B** and **C**, respectively.

As may be seen in Figs. 6 and S1, Cs(1) as well as Rb(1) (both interacting with the monodentate Pic^-) are situated almost symmetrically between the two opposite phenol rings of **1**, slightly above them and close to the centre of the corresponding CE. Three terminal carbon atoms of each aromatic unit are involved in the metal π-coordination, with those in the *p*-positions (i.e. C(4B) and C(20B)) being at much

[4]The CE conformations in the complexes **A**, **B** and **C**, similar to the geometry of crown 2 in **D**, are distorted from the conformation described by the sequence of O—C—C—O torsion angles as $g^+g^-g^+g^-g^+$ [25] (*g* stands for *gauche* angle), which is considered to be most energetically beneficial for 18-crown-6 ring. A detailed information on the CE conformations in these complexes is provided in Tables S1 and S2 in the Supplementary information.

TABLE IV Crystallographic data for the structures of $[Tl_2\mathbf{1}(Pic^-)(CH_3OH)]^+(Pic^-)\cdot CH_3OH$ (**A**), $[Cs_2\mathbf{1}(Pic)_2]$ (**B**) and $[Rb_2\mathbf{1}(Pic)_2]$ (**C**).

	A	**B**	**C**
Formula	$C_{62}H_{71}N_6O_{28}Tl_2$	$C_{60}H_{64}Cs_2N_6O_{26}$	$C_{60}H_{62}N_6O_{26}Rb_2$
Formula wt	1756.99	1550.99	1454.10
Temperature, K	203(2)	203(2)	203(2)
Wavelength, Å	0.71073	0.71073	0.71073
Crystal colour	Yellow	Yellow	Yellow
Crystal system	Monoclinic	Monoclinic	Monoclinic
Space group	$P2_1/a$	$P2_1/c$	$P2_1/a$
a (Å)	20.9559(6)	18.182(4)	18.1730(3)
b (Å)	11.4995(3)	21.326(4)	21.3150(2)
c (Å)	28.3682(10)	18.341(4)	18.3563(3)
α, °	90	90	90
β, °	106.217(4)	117.30(3)	117.218(2)
γ,°	90	90	90
V, Å^3	6564.2(3)	6320(2)	6323.13(16)
Z	4	4	4
D(calcd), Mg m^{-3}	1.778	1.630	1.527
μ, mm^{-1}	4.996	1.244	1.638
F(000)	3484	3136	2984
Crystal size, mm^3	0.39 × 0.33 × 0.27	0.47 × 0.34 × 0.21	0.45 × 0.35 × 0.19
θ range, °	4.61 to 30.68	4.58 to 30.97	4.57 to 32.65
h, k, l range	$-29 \le h \le 29$ $-15 \le k \le 16$ $-40 \le l \le 39$	$-26 \le h \le 16$ $-30 \le k \le 29$ $-23 \le l \le 24$	$-27 \le h \le 27$ $-32 \le k \le 31$ $-27 \le l \le 27$
Reflections collected	54,179	48,493	175,294
Independent reflections	17,630	17,283	21,563
R_{int}	0.0862	0.0689	0.0552
T (min; max)	0.298; 0.188	1.00000; 0.83391	1.00000; 0.83391
Refinement method	Full-matrix least-squares on F^2	Full-matrix least-squares on F^2	Full-matrix least-squares on F^2
GOF on F^2	1.087	0.795	1.123
R1/wR2 [$I > 2\sigma(I)$]	0.0758/0.0998	0.0347/0.0630	0.0781/0.1965
R1/wR2 (all data)	0.1904/0.1406	0.1194/0.0759	0.1408/0.2657
$\Delta\rho_{max}/\Delta\rho_{min}$, e Å^{-3}	1.832/−2.058	1.861/−0.803	3.395/−0.886

shorter distances to the neighbouring $Cs^+(Rb^+)$ cations than the two *m*-carbons in the same rings (Table III). Such a pattern is typical for the known Cs^+-complexes of **1** and its analogues [10,11]. The Cs(1)–C separations in **B** range from 3.319(3) to 3.662(4) Å and the Rb(1)–C distances in **C** are between 3.289(6) and 3.662(6) Å (mean value 3.5(1) Å for each of the complexes). However, it should be taken into account that the sum of the ionic radius for M^+ and van der Waals radius for C, $s_{M\text{-}C}$, is larger for Cs^+(3.39 Å) than for Rb^+(3.18 Å). Accordingly, Cs(1) approaches the *p*-carbon atoms C(4B) and C(20B) at distances comparable with s_{Cs-C}; while the analogous separations for Rb(1) are longer than s_{Rb-C}. Hence, in spite of the very similar structural parameters of **B** and **C**, $Cs^+\pi$-coordination with **1** is stronger than that for Rb^+. With the bidentate Pic^- involved, M(2) in both **B** and **C** is situated slightly farther and less symmetrically about the two opposite aromatic units than M(1) (see Table 3). The overall mean Cs–C distance in **B** is 3.6(1) Å (in agreement, in the nitrate complex **D**, this mean value is 3.6(2) Å [10]) and Rb–C distance in **C** is 3.5(2) Å.

The arrangement of Tl^+-containing structure **A** in the area of calixarene aromatics is distinctive from that in **B** and **C**. The position of both Tl(1) coordinated with Pic^- and Tl(2) bound with MeOH about the corresponding pairs of phenol rings is asymmetrical. Each of these metal ions resides noticeably closer to one of the aromatic units in the pair than to the other one (Fig. 5; Table III). This tendency is especially expressed for Tl(2). Thus, Tl(2) is bound efficiently with three neighbouring carbon atoms, C(3A), C(4A) and C(5A), for which the Tl(2)–C separations range from 3.089(7) to 3.387(7) Å (the mean value 3.2(1) Å is comparable with the s_{Tl-C} of 3.14 Å). At the same time, this thallium ion barely interacts with the opposite phenol ring, with the Tl(2)–C distances varying between 3.470(7) and 3.730(6) Å (mean value 3.6(1) Å). Such an asymmetry in Tl^+ location relative the two π-donor binding sites may be rationalised by the strong tendency of this soft electron acceptor for π-coordination that cannot be realised with the participation of both of the aromatic moieties because of the relatively small size of the cation. The overall mean Tl–C distance in this complex is 3.4(2) Å, which is smaller than the mean Cs–C and Rb–C distances in **B** and **C**, respectively.

The relative strength of the cation–π interactions in **A**, **B** and **C** may be characterised also by the effect they cause on the conformation of the calixarene moiety, i.e. mutual spatial orientation of the phenol rings. Although no major variation in the *1,3-alternate* conformation of **1** may be expected, the simultaneous π-coordination of a metal ion with the pair of opposite aromatic units may somewhat decrease the dihedral angle (θ) between the mean planes for

these rings. The magnitude of θ in **A** is 22.19 and 24.20° about Tl(1) and Tl(2), respectively. In **B** and **C**, the analogous pairs of dihedral angles are 26.94 and 26.37°, and 25.20 and 26.78°, respectively. Accordingly, the mean values of θ in these complexes vary from 23.2° in **A** to 26.6° in **B** and 26.0° in **C**, which evidently reflects a stronger attraction of the π-coordinated phenol rings to Tl^+ than to Rb^+ and Cs^+.

In summary, a comparative analysis of the crystal structures **A**, **B** and **C** as well as the solution ^{1}H NMR studies revealed a stronger involvement of Tl^+ in π-coordination with the aromatic framework of **1** than for Rb^+ and Cs^+. The structural data suggest that complexation of a soft electron acceptor Tl^+ with **1** is driven by the cation–π interactions rather than coordination with hard CE oxygen donors. On the contrary, for hard Cs^+ and Rb^+, the metal–oxygen bonding plays the principal role which is supported by the cation–π interactions.

EXPERIMENTAL

Compound **1** was prepared as described earlier [14]. Thallium(I) carbonate (99.9%) from Aldrich was used as received from the supplier. CAUTION! Compounds of thallium(I) are poisonous and may cause severe health effects if ingested, inhaled or adsorbed through skin. Metal picrates were prepared analogous to the published procedure [26]. CAUTION! Metal picrates (AgPic and TlPic especially!) are potential explosive hazards which are sensitive to heat, friction or impact. ACS-grade chloroform from Fisher, prior to use in the extraction experiments, was washed with deionised water. ^{1}H NMR spectra were recorded with Bruker Avance 400.13 MHz spectrometer at 293 K. Chemical shifts were measured against TMS as internal standard. UV–Vis spectra were obtained with a Shimadzu UV-2101PC scanning spectrophotometer. Solvent extraction samples were shaken with Glas-Col® Multi-Pulse vortexer.

Solvent Extraction of Metal Picrates by 1

4.0 ml of 0.10 mM aqueous solution of metal picrate and 4.0 ml of **1** (varying concentration) in $CHCl_3$ was placed in a plastic metal-free centrifuge tube, vortexed for 30 min, centrifuged and phases separated. The absorbance of the aqueous phase before and after extraction at 357 nm was measured and the percent extraction calculated from the difference.

Preparation of Dinuclear Complexes Tl_2**1**$(Pic)_2$, Rb_2**1**$(Pic)_2$ And Cs_2**1**$(Pic)_2$

0.050 g (0.060 mmol) of **1** was stirred at room temperature with 0.12 mmol of the corresponding metal picrate in 4 ml of chloroform–methanol (4:1) until complete dissolution of the solid. Single crystals suitable for X-ray crystallography were obtained by slow diffusion of diethyl ether in the above chloroform–methanol solution. For use in the ^{1}H NMR studies, the crystals were filtered, washed with cold diethyl ether, dried *in vacuo* and dissolved in $CDCl_3$. (The completeness of removal of residual methanol from the samples was verified by the absence of the corresponding signals in the ^{1}H NMR spectra in $CDCl_3$)

X-ray Crystallography

A crystal of colour and dimensions indicated in Table IV was mounted on a glass fibre using a small amount of epoxy cement. Data were collected on an Oxford Diffraction Gemini R CCD diffractometer. The crystals were irradiated using Mo K_α radiation ($\lambda = 0.71073$) with 1° scans. An Oxford Diffraction Cryojet XL low-temperature device was used to keep the crystals at a constant temperature of 203(2) K during data collection. Crystallographic data for the complexes are presented in Table 4.

Data collection was performed and the unit cell was initially refined using CrysAlis CCD, Version 1.171.31.8 [27]. Data reduction was performed using CrysAlis Red, Version 1.171.31.8 [28] and XPREP v6.12 [29]. Corrections were applied for Lorentz polarisation. Empirical absorption correction was applied using spherical harmonics, implemented in the SCALE3 ABSPACK scaling algorithm [28]. The structure was solved and refined with the aid of the programs in the SHELXTL-plus [v6.10] system of programs [30]. The full-matrix least-squares refinement on F^2 included atomic coordinates and anisotropic thermal parameters for all non-H atoms. The H atoms were included using a riding model.

Crystallographic data for the structures reported in this paper have been deposited with the Cambridge Crystallographic Data Centre as supplementary publications nos. CCDC 656497 (structure **A**), 656496 (**B**) and 656494 (**C**).

CONCLUSIONS

1,3-Alternate calix[4]arene-bis(crown-6) (**1**) demonstrates a high selectivity for Tl^+ over other unicharged metal ions, including Cs^+ and Rb^+. This phenomenon is attributed to stronger tendency of soft Tl^+ for π-coordination with aromatic rings of the calixarene moiety. As evident from the solution ^{1}H NMR and crystal X-ray data, cation–π interactions play a major role in the complex formation of Tl^+ with **1**.

Acknowledgements

This research was supported by Howard University (Grant NF05/14). R.J.B. wishes to acknowledge the NSF-MRI program for funds to purchase the X-ray diffractometer.

References

[1] *Calixarenes for Separations*; Lumetta, G.J., Rogers, R.D., Gopalan, A.S., Vicens, J., Eds.; American Chemical Society: Washington, DC, 2000; ACS Symposium Series 757.
[2] Ludwig, R. *Fresenius J. Anal. Chem.* **2000**, *367*, 103.
[3] Ikeda, A.; Shinkai, S. *Chem. Rev.* **1997**, *97*, 1713.
[4] Matthews, S.E.; Rees, N.H.; Felix, V.; Drew, M.G.B.; Beer, P.D. *Inorg. Chem.* **2003**, *42*, 729.
[5] Yajima, S.; Yoshioka, N.; Tanaka, M.; Kimura, K. *Electroanalysis* **2003**, *15*, 1319.
[6] Kimura, K.; Tatsumi, K.; Yokoyama, M.; Ouchi, M.; Mocerino, M. *Anal. Commun.* **1999**, *36*, 229.
[7] Baklouti, L.; Harrowfield, J.; Pulpoka, B.; Vicens, J. *Mini-Rev. Org. Chem.* **2006**, *3*, 355.
[8] Ungaro, R.; Casnati, A.; Ugozzoli, F.; Pochini, A.; Dozol, J.F.; Hill, C.; Rouquette, H. *Angew. Chem. Int. Ed. Engl.* **1994**, *33*, 1506.
[9] Casnati, A.; Pochini, A.; Ungaro, R.; Ugozzoli, F.; Arnaud, F.; Fanni, S.; Schwing, M.-H.; Egberink, R.J. M.; de Jong, F.; Reinhoudt, D.N. *J. Am. Chem. Soc.* **1995**, *117*, 2767.
[10] Asfari, Z.; Naumann, C.; Vicens, J.; Nierlich, M.; Thuery, P.; Bressot, C.; Lamare, V.; Dozol, J.-F. *New J. Chem.* **1996**, *20*, 1183.
[11] Thuery, P.; Nierlich, M.; Lamare, V.; Dozol, J.-F.; Asfari, Z.; Vicens *J. Inc. Phenom. Macrocycl. Chem.* **2000**, *36*, 375.
[12] Dozol, J.-F.; Simon, N.; Lamare, V.; Rouquette, H.; Eymard, S.; Tournois, B.; De Marc, D.; Macias, R.M. *Sep. Sci. Technol.* **1999**, *34*, 877.
[13] Moyer, B.A.; Birdwell, J.F., Jr.; Bonnesen, P.V.; Delmau, L.H. In *Macrocyclic Chemistry – Current Trends and Future*; Gloe, K., Ed.; Springer: Dordrecht, 2005; pp 383–405.
[14] Asfari, Z.; Bressot, C.; Vicens, J.; Hill, C.; Dozol, J.F.; Rouquette, H.; Eymard, S.; Lamare, V.; Tournois, B. *Anal. Chem.* **1995**, *67*, 3133.
[15] Arnaud-Neu, F.; Asfari, Z.; Souley, B.; Vicens, J. *New J. Chem.* **1996**, *20*, 453.
[16] Hill, C.; Dozol, J.F.; Lamare, V.; Rouquette, H.; Tournois, B.; Vicens, J.; Asfari, Z.; Bressot, C.; Ungaro, R.; Casnati, A. *J. Inclusion Phenom. Mol. Recognit. Chem.* **1994**, *19*, 399.
[17] Haverlock, T.J.; Bonnesen, P.V.; Sachleben, R.A.; Moyer, B.A. *J. Incl. Phenom. Macrocycl. Chem.* **2000**, *36*, 21.
[18] Talanov, V.S.; Talanova, G.G.; Gorbunova, M.G.; Bartsch, R.A. *J. Chem. Soc., Perkin Trans. 2* **2002**, 209.
[19] Roper, E.D.; Talanov, V.S.; Gorbunova, M.G.; Bartsch, R.A.; Talanova, G.G. *Anal. Chem.* **2007**, *79*, 1983.
[20] Casnati, A.; Ungaro, R.; Asfari, Z.; Vicens, J. In *Calixarenes 2001*; Asfari, Z., Bohmer, V., Harrowfield, J., Vicens, J., Eds.; Kluwer Academic Publications: Dordrecht/Boston/London, 2001; Chapter 20, pp 365–384.
[21] Izatt, R.M.; Pawlak, K.; Bradshaw, J.S.; Bruening, R.L. *Chem. Rev.* **1991**, *91*, 1721.
[22] Pauling, L. *The Nature of the Chemical Bond*; 3rd ed.; Cornell University Press: Ithaca, New York, 1960.
[23] Talanova, G.G.; Elkarim, N.S. A.; Talanov, V.S.; Hanes, R.E.; Hwang, H.-S.; Bartsch, R.A.; Rogers, R.D. *J. Am. Chem. Soc.* **1999**, *121*, 11281.
[24] Thuery, P.; Nierlich, M.; Arnaud-Neu, F.; Souley, B.; Asfari, Z.; Vicens, J. *Supramolecular Chem.* **1999**, *11*, 143.
[25] Fyles, T.M.; Gandour, R.D. *J. Incl. Phenom.* **1993**, *12*, 313.
[26] Coplan, M.A.; Fuoss, R.M. *J. Phys. Chem.* **1964**, *68*, 1177.
[27] CrysAlis CCD, Oxford Diffraction Ltd, Version 1.171.31.8 (release 12-01-2007 CrysAlis171.NET) (compiled Jan 12 2007,17:49:11).
[28] CrysAlis RED, Oxford Diffraction Ltd, Version 1.171.31.8 (release 12-01-2007 CrysAlis171.NET) (compiled Jan 12 2007,17:49:11).
[29] Bruker, XPREP v6.12. Bruker AXS Inc., Madison, Wisconsin, USA, **2001b**.
[30] Bruker, SHELXTL v6.10. Bruker AXS Inc., Madison, Wisconsin, USA, **2000**.

SUPPLEMENTARY INFORMATION

Supplementary information available: structure diagram for complex $[Rb_2\mathbf{1}(Pic)_2]$ (**C**); crystal packing for **A**, **B** and **C**; structural information on the CE conformations in **A**, **B** and **C**; list of selected torsion angles.